Hydrothermal Destruction and Defluorination of Trifluoroacetic Acid (TFA)

*Conrad Austin [a,b], Anmol L. Purohit [a], Cody Thomsen [a, b], Brian R. Pinkard [a, b], Timothy J. Strathmann [c], Igor V. Novosselov [a] **

[a] University of Washington, Mechanical Engineering Department, Seattle, WA 98195

[b] Aquagga, Inc., Tacoma, WA 98402

[c] Colorado School of Mines, Civil and Environmental Engineering Department, Golden, CO 80401

* Corresponding Author: ivn@uw.edu; +1 206 543-5248

ORCID [0000-0002-6347-7450]

Abstract

Per- and polyfluoroalkyl substances (PFAS) have received increased attention due to their environmental prevalence and threat to public health. Trifluoroacetic acid (TFA) is an ultra-short-chain PFAS and the simplest perfluorocarboxylic acid (PFCA). While the US EPA does not currently regulate TFA, its chemical similarity to other PFCAs and its simple molecular structure make it a suitable model compound for studying the destruction of PFAS. We show that hydrothermal processing in compressed liquid water degrades TFA at relatively mild conditions (T = 150 – 250 ˚C, P < 30 MPa), initially yielding gaseous products, such as CHF_3 and CO_2, that naturally aspirate from the solution. Alkali amendment (*e.g.*, NaOH) promotes the mineralization of CHF_3, yielding dissolved fluoride, formate, and dissolved carbonate species as final products. Fluorine and carbon balances are closed using Raman spectroscopy and fluoride ion selective electrode measurements for experiments performed at alkaline conditions, where gas yields are negligible. Qualitative FTIR gas analysis allows for establishing the degradation pathways; however, the F-balance could not be quantitatively closed for experiments without NaOH amendment. The kinetics of TFA degradation under hydrothermal conditions are measured, showing little to no dependency on NaOH concentration, indicating that the thermal decarboxylation is a rate-limiting step. A proposed TFA degradation mechanism motivates additional work to generalize the hydrothermal reaction pathways to other PFCAs.

Keywords: PFAS, trifluoroacetic acid, fluoroform, hydrothermal, alkaline, reaction kinetics

Synopsis: TFA degradation under mild hydrothermal conditions yields gaseous CHF_3 and CO_2, and alkali amendment rapidly mineralizes organic fluorine.

1 Introduction

1.1 Background

Per- and polyfluoroalkyl substances (PFAS) are a group of recalcitrant compounds whose widespread contamination, environmental persistence, and toxicity have triggered public health concerns [1, 2]. Three PFAS, perfluorooctanesulfonic acid (PFOS), perfluorooctanoic acid (PFOA), and perfluorohexanesulfonic acid (PFHxS), have been added to the Stockholm Conventions list of persistent organic pollutants (POPs) [3], and the US EPA recently proposed maximum contaminant levels (MCLs) for six PFAS, including PFOS, PFOA, PFHxS, perfluorononanoic acid (PFNA), perfluorobutanesulfonic acid (PFBS), and hexafluoropropylene oxide-dimer acid (HFPO-DA), also known as GenX.

Though not on the list of regulated compounds, trifluoroacetic acid (TFA) is one of the most common perfluorinated chemicals; as of 2006, between 1 and 10 million lbs. are manufactured or imported annually to the United States [4]. TFA is used as a solvent, an acid catalyst, and a reagent in trifluoromethylation reactions. The trifluoromethyl group (CF_3-) is also common in many pharmaceutical compounds such as fluoxetine (Prozac®), agrochemicals (e.g., trifluralin [5, 6]), refrigerants (e.g., R-134a), and most PFAS. Environmental degradation of these compounds and longer-chain PFAS can yield TFA; it has also been detected as a byproduct of PFAS treatment in supercritical water oxidation (SCWO) [7], plasma-based treatment [8], hydrothermal treatment [9, 10] and low-temperature treatment of PFCAs [11]. TFA is the smallest and simplest PFCA molecule and is likely to follow similar reactivity as its longer chain analogues, which is attractive for elucidating the primary reaction mechanisms of PFCAs.

Several end-of-life PFAS destruction technologies have been investigated, including photocatalytic degradation [12], sonochemical destruction [13], plasma-based treatment [8],

electrochemical oxidation [14, 15], and hydrothermal technologies [16]. Treatment methods that rely on the partitioning behavior of PFAS do not readily degrade TFA. The hydrothermal approaches treat the entire fluid volume and show greater promise; however, the reaction rates and the routes for TFA and longer-chain PFCA destruction are only partially understood.

While LC-MS/MS methods are well established for PFAS analysis, rapid spectroscopic analysis techniques can significantly expedite research and facilitate quantitative reaction kinetic studies. Raman spectroscopy is well-suited for analyzing aqueous mixtures, as water has a weak Raman spectrum, allowing for the rapid identification and quantification of mixture constituents. Quantitative Raman spectroscopy relies on the principle that the magnitude of a molecule's Raman signal is directly proportional to its molar concentration in the sampling volume. While Raman spectroscopy was not previously used for studying the chemical kinetics of PFAS degradation, the spectra peak heights or peak areas can be used to quantify species concentrations of parent compounds and byproducts of the reaction [17]. These data can be used to determine the chemical reaction kinetics, as previously shown for organic acids [18], alcohols [19, 20], and chemical agent surrogates [21]. The signal calibration and spectra deconvolution can be challenging for low concentrations of analytes and complex mixtures, such as intermediates of the decomposition of complex molecules [22]. Raman scattering is a weak phenomenon; thus, PFAS concentrations must be relatively high (>mg/L) to generate useful data. TFA decomposition is particularly well-suited for analysis by Raman spectroscopy due to the limited number of potential decomposition products, their clear Raman signals, and their high solubility in the liquid phase.

Hydrothermal methods have been used to destroy PFAS in subcritical water under alkaline conditions and supercritical water under oxidative conditions [7, 15, 23-25]. Hydrothermal alkaline treatment (HALT) in batch reactors has been shown to destroy and defluorinate PFAS

compounds in various matrices, including AFFF [26, 27], spent GAC [28], contaminated groundwater [29], and foam fractionate [30]. The literature suggests second-order rate constants for PFOA destruction and proposed second-order rate constants for PFOS at fixed T = 350 ˚C [9, 24]. TFA is a suitable model compound for studying the reaction kinetic rates and reaction mechanisms; these can be extrapolated for more complex PFCAs (*e.g.*, PFOA, PFNA).

Continuous flow HALT (CF-HALT) was demonstrated to treat PFAS-impacted fire training pit water [31]. However, outside of this case study, the rates and the kinetic pathways in the CF-HALT process have not been presented in the literature. Continuous flow hydrothermal systems are advantageous in practical applications and enable real-time process monitoring and control [32]. Related to PFAS treatment, continuous flow SCWO reactors show significantly higher destruction efficiencies of neat PFAS [7, 15] than batch reactor experiments [33]. One possibility for higher destruction rates is that mixing phenomena in continuous flow regimes provide better heat and mass transfer required for reactions. At the same time, the bulk solution remains in the liquid phase [34]. Additionally, a high surface-to-volume (S/V) ratio in the tubular reactors may be responsible for catalytic wall effects, increasing reaction rates.

Motivated by the need to find effective PFAS treatment technologies and hypothesizing that the decomposition pathways of TFA are analogous to the longer chain PFCAs, we studied TFA decomposition in compressed subcritical water with and without alkali amendment. Two continuous flow systems were used to evaluate the effect of the S/V ratio on the reaction rate. Fluorine and carbon balance are tracked by combining Raman spectroscopy and fluoride ion selective electrode (ISE). To capture byproducts that could be separated from the bulk liquid and exist in the headspace, gaseous products were analyzed by Fourier transform infrared (FTIR)

spectroscopy. The data were used to measure reaction kinetics and establish the mechanisms controlling TFA degradation and mineralization.

2 Materials & Methods

2.1 Experimental Apparatus: Continuous Flow Hydrothermal Reactors

Two continuous-flow, tubular hydrothermal reactors with different surface-to-volume (S/V) ratios were used for the experiments described herein. The two reactors were designed to achieve the same operating conditions, *e.g.*, temperature, pressure, and residence time (τ_{res}), with different form factors and heating strategies. Testing in the two systems assesses the potential effects of surface chemistry and informs the design of scaled-up hydrothermal reactors. Gas and liquid effluent collected from both reactors were used to measure reaction rates and elucidate transformation pathways. Reactor 1 was used to gather liquid samples. Reactor 2 operates with a much higher throughput, generating more gaseous products during an experiment; the gas samples from Reactor 2 are presented. Figure 1 shows the conceptual approach used in the study.

2.1.1 Reactor 1

Reactor 1 uses a positive displacement SSI (Teledyne, LS-Class) HPLC pump to introduce the feedstock (premixed TFA-NaOH solution) into an Inconel 600 (INC600) tubular reactor section, with a length of 10 m, OD ~ 3.18 mm ($1/8^{th}$ inch tubing), internal volume 4.2mL, and a S/V ~ 26.3 cm^{-1}, see Figures S1 and S3 The heated reactor section is coiled and submerged in a heated sand bath, held at a set temperature using a proportional–integral–derivative (PID) controller. The type-K thermocouples measure the temperature in the sand bath and the reactor tubing. The measurements of the reactor wall upstream and downstream of the coiled section confirm that the reactor operates at near-isothermal conditions ($\Delta T < 5\ ^{o}C$), appropriate for studying the reaction kinetic rates. After exiting the heated section, the reaction products are

rapidly cooled in a quenching section where the INC600 tubing is submerged in room-temperature water. After quenching, products are throttled across a back-pressure regulator (BPR) and enter the gas-liquid separator. The effluent is collected in glass scintillation vials. A 2 mL aliquot is removed from the scintillation vial and put into a 2 mL polypropylene microcentrifuge tube. The naturally aspirated gaseous products are collected in Tedlar™ bags.

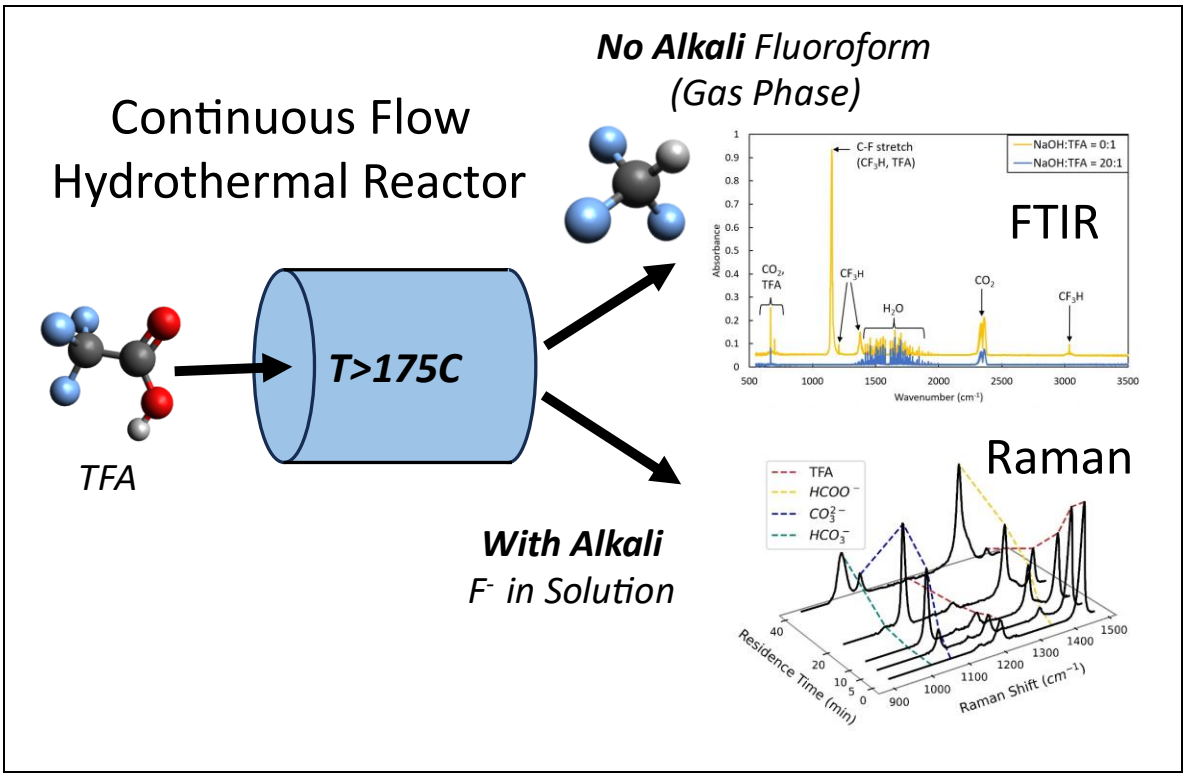

Figure 1: Conceptual diagram of the approach. Aqueous TFA solution is processed in a continuous flow hydrothermal reactor at T > 175 °C, P = 25 MPa. Gaseous and liquid products were collected and characterized to elucidate the reaction mechanism.

2.1.2 Reactor 2

A separate, larger flow rate reactor (Reactor 2) was used to evaluate the effect of the S/V ratio on the kinetic rates of TFA degradation and the potential for scale-up. The throughput of ~0.5 - 3 gph (0.032 - 0.19 lpm) is based on the pump performance and heat exchanger design. A PFD and the system images are shown in Figures S2 and S4. A high-pressure diaphragm metering pump (LEWA, Leonberg, Germany) feeds a premixed TFA-NaOH solution through the reactor

assembly, consisting of a counter-flow tube-in-tube recuperative heat exchanger and a welded Inconel reactor section, with a S/V = 1.57 cm^{-1}. The influent is preheated in the heat exchanger before it enters the reactor heated by three resistive band heaters. Type K thermocouples are placed inside thermowells to measure fluid temperature and are used in PID controls. The effluent is passed through a heat exchanger and cooled below 100 °C. The solution is throttled across the BPR; the effluent stream is passed through a gas/liquid separator, the gas is collected in a Tedlar™ bag, and the liquid samples are collected in 50 mL centrifuge tubes. The τ_{res} is found using an approximated density at a given temperature and pressure for the internal volume of this reactor (627 mL). The τ_{res} in the heat exchanger during temperature ramp-up and cool-down is not considered in the analysis of kinetic rates.

2.1.3 Reagents

Deionized (DI) water (resistivity, ρ = 18.2 MΩ-cm) from ELGA PURELAB® Option-Q lab water purification system was used for preparing all stock solutions. TFA (>99%, Thermo Fisher Scientific) was used to prepare stock solutions for testing without further purification. 10 M-NaOH solution (Supelco) was used for reagent preparation. LC/MS grade methanol (>99.9%, Optima), LC/MS grade water (Optima), and HPLC grade ammonium acetate (>98%, Fisher) were used for LC-MS/MS samples.

2.2 Experimental Procedures

Experimental procedures were the same for both reactor systems. The reactor was heated to the experimental temperature while pumping DI water at the desired flow rate. Once the set temperature was reached, the premixed TFA-NaOH solution was introduced. The samples were collected after a prescribed time delay, allowing the reactants and products to flow through the reactor and reach a steady-state effluent profile. The required sampling delay is based on the τ_{res}

distribution curve, characteristic of the laminar flow regime, and considering the fluid density in the hot and cold sections of the reactor [35]. Both reactors were operated in the T = 150 - 275 °C range and at a pressure of 25 MPa to maintain the compressed liquid phase. The τ_{res} = 5- 40 min was set by adjusting the pump flow rates. The TFA inlet concentration was 0.02 M (2.28 g/L) or 0.1 M (11.4 g/L) for Reactor 1 and 0.01 M (1.14 g/L) for Reactor 2. The molar concentration of NaOH was varied in the 0 to 2 M range, corresponding to NaOH: TFA molar ratios of 0:1, 4:1, and 20:1. SI Table 1 shows the experimental matrix.

2.3 Product Analysis

Raman Spectroscopy was performed on the liquid effluent. A MarqMetrix® (AIO-M72) Raman system (MarqMetrix, Seattle, WA) was used with a custom 1/8" sapphire BallProbe®. A 785 nm, 450 mW laser was used with an integration time of 10 s. The detector spectral range is 200-3100 cm^{-1} with 8 cm^{-1} resolution (MarqMetrix Inc., Seattle, WA). In-house code was used to automatically subtract the spectrum's fluorescent baseline and deconvolute peaks [18, 22]. Additional details on the methods and calibration are shown in Figures S5 and S6. Liquid effluent was also quantified using a quadrupole tandem mass spectrometer with a 2795 Alliance HT LC system (LC-MS/MS; Waters, Milford, MA). The LC was equipped with a Zorbax Eclipse XDB-C18 column (Agilent, Santa Clara, CA). A calibration curve was obtained in the 0.05-50 ppb range using the unlabeled TFA, sodium salt standard (Cambridge Isotope, Tewksbury, MA). Each effluent sample was diluted with LC-MS grade methanol (60%) and water (40%). The mobile phase consisted of 10 mM ammonium acetate in water and 10 mM ammonium acetate in methanol. LC-MS/MS protocols were previously reported [7].

Fluoride analysis was performed using fluoride ISE (Orion, 9609BNWP). All samples were diluted in water and mixed with total ionic strength adjustment buffer 2 (TISAB 2) 50% (v/v).

Calibration was performed before each experimental set using five dilutions in the 25 – 7000 µg/L range. The pH was measured before and after the experiments see Figure S7.

Gas analysis was performed by FTIR (Perkin Elmer Frontier, Waltham, MA) equipped with a gas cell (100x38 mm), Pike Technologies (Fitchburg, WI). The sample peaks in the mid-IR range (4000 – 1000 cm^{-1}) were scanned 30 times at a resolution of 0.5 cm^{-1}. The CaF_2 cell mirror limited analysis to $\lambda > 1000$ cm^{-1}. The gas sample was diluted ~1000x with argon and nitrogen to avoid saturation of spectra. A laboratory blank sample was analyzed before every sample, and the gas cell was flushed with air between runs.

3 Results & Discussion

3.1 Sample Analysis

A limited number of potential byproducts in the TFA decomposition allows for deconvolution of spectra of Raman and FTIR spectra [19]. Figure 2 (a) shows the Raman spectra for liquid effluent, NaOH:TFA = 4:1 (stoichiometric conditions for TFA mineralization), T = 200 °C and varied residence time; four species were detected in the effluent: TFA, formate ($HCOO^-$), carbonate (CO_3^{2-}), and bicarbonate (HCO_s^-). As τ_{res} increases, the TFA peaks decrease, and formate, carbonate, and bicarbonate peaks increase. The ratio HCO_3^-/CO_3^{2-} increases with reaction time due to NaOH consumption, as shown in Figure 2(a). At the NaOH:TFA = 20:1 condition (NaOH excess), the HCO_3^- is absent in the effluent as the pH >> 10.3 (pK_{a2} of carbonic acid). Formate was also observed in the effluent, in agreement with previous work on CHF_3 / NaOH systems [36, 37].

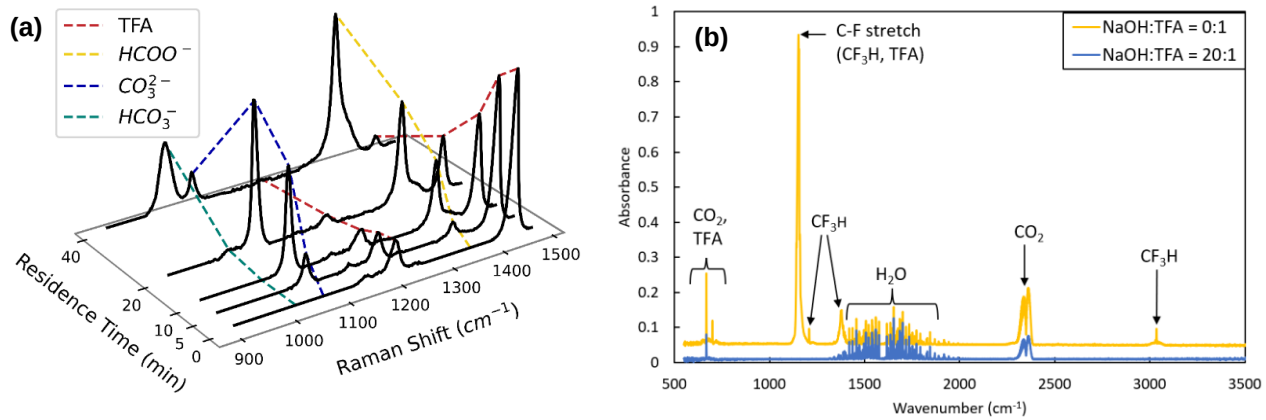

Figure 2: TFA decomposition products, τ_{res} ~ 10min, T =200°C: (a) Raman spectra for the liquid samples 4:1 NaOH/TFA. (b) FTIR spectra for gas samples, NaOH / TFA = 0:1(no NaOH), show the presence of TFA, CO_2, and CHF_3; NaOH / TFA = 20:1 (NaOH excess) shows only CO_2 emissions. The 0:1 case FTIR spectra are offset for presentation purposes.

Figure 2(b) shows the typical FTIR spectra of the gaseous sample for TFA degradation for 0:1 TFA/NaOH case (0 M and 0.00875 M) and 20:1 (0.175 M and 0.00875 M). Three gases were identified: TFA, CHF_3, and CO_2. The peaks at λ = 1150, 1209, 1380, and 3035 cm^{-1} indicate the presence of fluorocarbons using the HITRAN and NIST databases. The 1150 and 1209 cm^{-1} peaks are associated with C-F stretches, indicating TFA vapors or CHF_3 presence. The fluoroform is best identified by 1380 cm^{-1} and 3050 cm^{-1} peaks as that C-H bend and stretch are specific only to CHF_3. The TFA-specific peaks are associated with C=O stretch at 1850 $^{cm-1}$, and CO_2 has a specific double peak at ~2350 cm^{-1}. These cases demonstrate the production of CHF_3 by hydrothermal decarboxylation of TFA and mineralization by NaOH in a high pH environment. For the same level of sample introduced to the FTIR, CO_2 peaks are lower in the high NaOH condition, where carbon was partially bound in water-soluble products. Note that Raman spectra show the presence of carbonate ions as a final product at high pH conditions, while lower pH cases show both carbonate and bicarbonate ions, see Figure 2(a).

3.2 Carbon and fluorine balance

Figure 3 shows the summed yields (%mol) for carbon- and fluorine-containing species measured in the liquid phase. Gaseous carbon- and fluorine-containing species were identified but not

analyzed quantitatively; thus, they were not incorporated into the mass balance. Figure 3(a) and (b) show TFA degrades without alkaline amendment at T ~200 °C; inorganic carbon and fluoride from the degraded TFA was not detected in the liquid phase. The carbon and fluorine from TFA degradation are present in gaseous products as CO_2 and CHF_3, as seen in the FTIR spectra in Figure 2(b).

Figure 3(c) and (d) show that a stoichiometric addition of NaOH yields full recovery of carbon and fluorine in the liquid effluent. The fluoride balance is close to 100% for all tested τ_{res}, organic fluorine products were not detected by FTIR in the gaseous phase. The balance of carbon-containing products (CO_3^{2-} and HCO_3^-) varies during the reaction with a change in pH (as the NaOH is being depleted), see Figure 2, and the final ratio depends on the effluent's pH. Formation of formate has been previously reported as the reaction product of fluoroform with NaOH [36, 37]. Previous studies also report CO as a product; however, none was detected in this study. Note that LC/MS/MS analysis for selected experimental conditions of TFA concentration in the liquid effluent closely matches the Raman measurements, see Table 1.

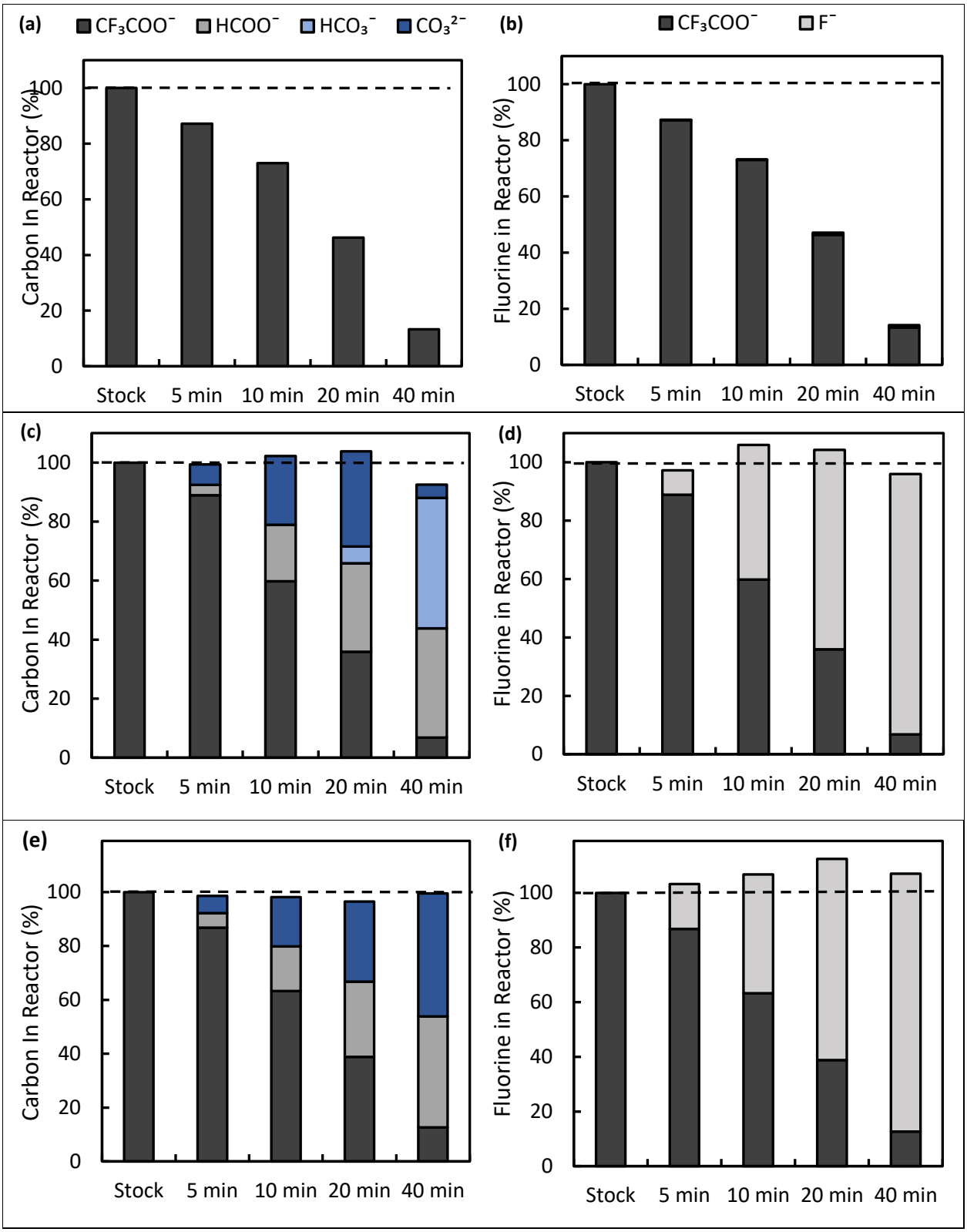

Figure 3: Aqueous phase C- and F- balance vs. τ_{res}, as measured by Raman and F-ISE in the liquid product. The initial NaOH concentration: 0 M NaOH (a, b), 0.4 M NaOH (c, d), and 2 M NaOH (e, f). Reaction conditions 0.1 M TFA, T = 200 ºC.

Table 1: Comparison of sample concentrations in Reactor 1 runs at T = 200 ˚C using LC/MS-MS and Raman Spectroscopy of the liquid effluent.

NaOH (M)	Residence Time (min)	Conc. TFA by Raman (M)	Conc. TFA by LC/MS-MS (M)	Percent Difference (%)
0.4	10	0.063	0.054	16.2
0.4	5	0.094	0.085	10.1
0	10	0.074	0.070	4.9

3.3 TFA destruction kinetics

Comparing the TFA destruction data from C- and F- mass balances, shown in Figure 3, the increase in NaOH concentration does not appear to affect the rate of TFA disappearance. Thus, a two-step global TFA mechanism in the NaOH-amended HALT environment can be proposed: (i) a rate-determining thermal decarboxylation of TFA yielding CHF_3 and CO_2, followed by (ii) CHF_3 mineralization by reaction with OH^-:

$$CF_3COOH \rightarrow CF_3H + CO_2 \quad \text{(R1)}$$

$$CF_3H + 4NaOH \rightarrow 3NaF + HCOONa + 2H_2O \quad \text{(R2)}$$

We anticipate that other alkali amendments will likely have a similar effect to NaOH; however, these were not investigated here.

The R1 reaction rate was previously investigated, most notably by Auerbach et al. [38] in ethylene glycol and Belsky et al. [39] in high-pressure water (P = 275 bar). Both studies report that TFA thermally degrades, yielding CHF_3 and CO_2 at T > 180 ˚C. The study by Belsky et al. is especially relevant as we can (i) extend the alkaline concentration range and (ii) compare the reaction rate from their Ti and 316 SS custom flow cell reactors [40] to data from our tubular INC600 reactor, S/V = 53.3 cm^{-1}.

The rates of fluoroform mineralization (step R2) were not directly quantified in this work. By itself, fluoroform is thermally stable up to T ~ 900 ˚C as shown in shock tube experiments [41]; however, fluoroform can be degraded at T ~ 600˚C by catalytic hydrolysis in the presence of water

vapor [42]. Moreover, in the presence of alkali, the reaction has been reported to occur at T ~ 150 ˚C [36, 37], which is lower than the temperature required for TFA decarboxylation (step R1). Our experiments are consistent with these findings, e.g., the addition of 0.4 M NaOH leads to stoichiometric formation of fluoride ion and a closed fluorine mass balance (100% ± 6%) for all tested conditions, indicating that the initial fluoroform reaction product from TFA reacts rapidly with OH^-, preventing its buildup and release from the reactor.

The first-order kinetic rate for hydrothermal decarboxylation ($F_3COOH \rightarrow CF_3H + CO_2$) was determined using an Arrhenius approach, see Figure 4 (a). The rates for Reactor 1 were derived using the data from three sets of experiments over the range of NaOH concentration (0 – 2M) corresponding to stoichiometric ratios of NaOH: TFA (0:1, 4:1, 20:1). In our experiments, the degradation rate for the parent TFA did not depend on the NaOH concentration and the best fit for Arrhenius rate constant, $k = A\, e^{\frac{-E_a}{RT}}$, is obtained with activation energy, E_a = *191.1 ± 7.8 kJ/mol,* and pre-exponential constant, *A = 40.82 ± 1.97* s^{-1}, where *R* is the gas constant.

Figure 4(b) shows the Reactor 1 and 2 data, the TFA decarboxylation rates, and the TFA thermal degradation rates previously measured in ethylene glycol [38] and hydrothermal Ti and 316 SS [39] reactor are in excellent agreement with our data, indicating that the TFA decomposition rate has little to no dependency on reaction media, wall material, or the amendments. To evaluate possible catalytic effects of Inconel, the data from Reactor 1 (S/V = 26.3 cm^{-1}) and Reactor 2 (S/V = 1.57 cm^{-1}) were compared. Figure 4(b) shows Reactor 1 having a lower apparent rate; however, it should be noted that τ_{res} for Reactor 2 did not include the time the liquid spent in the recuperative heat exchanger during the preheat to operating temperature and cool down to the temperature, so the apparent faster TFA destruction in Reactor 2 is likely due to the "shoulder effect" in the temperature profile as a function of the flow time. The agreement with Belsky et al.

from Ti and 316 SS reactors [39] further supports the conclusion that the hydrothermal decarboxylation step ($F_3COOH \rightarrow CF_3H + CO_2$) does not depend on wall properties.

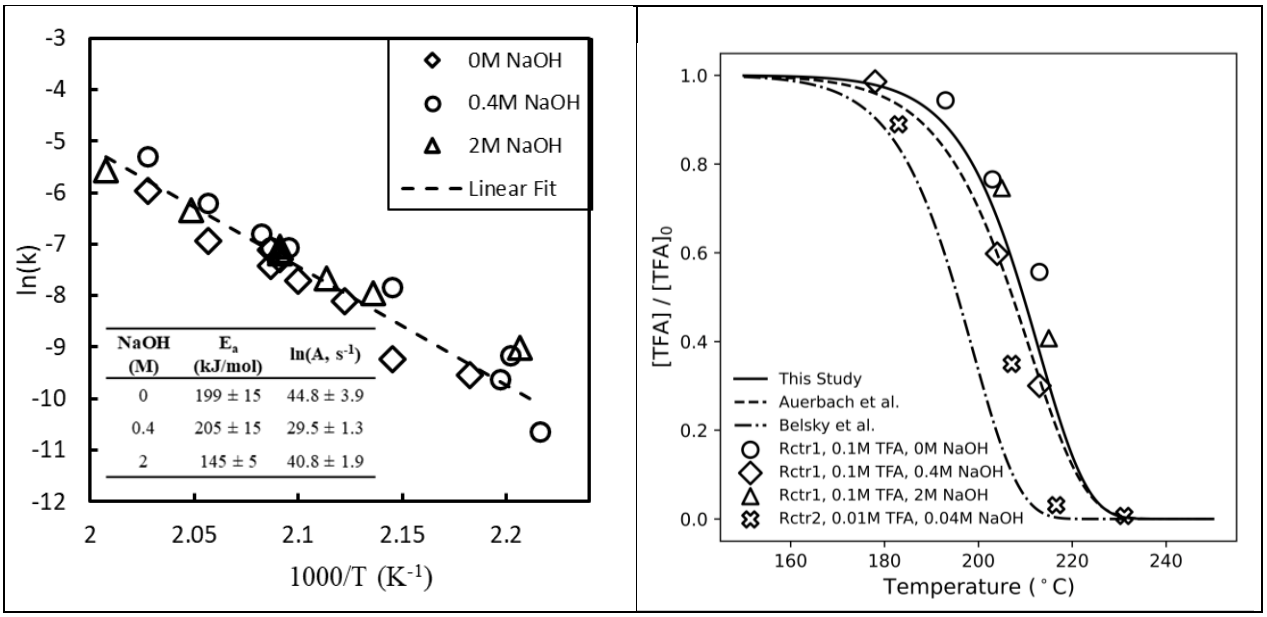

Figure 4: Arrhenius plot of TFA thermal degradation in hot alkaline liquid water. Reactor 1 has kinetics for NaOH:TFA stoichiometric ratios of 0:1 and 4:1. Reactor 2 has a much lower surface area to volume ratio to test any potential catalytic effect of the reactor wall materials.

3.4 Reaction Mechanism

In the absence or with sub-stoichiometric addition of alkaline, the hydrothermal decarboxylation step leads to the formation of gaseous CHF_3 and CO_2 and water-soluble inorganic carbon products CO_3^{2-} and HCO_3^-. A rate-determining thermal decarboxylation yields CO_2 and a CF_3^- carbanion species, the latter which rapidly abstracts a proton from water to form fluoroform (CHF_3). This product is volatile and will readily aspirate from neutral or acidic pH solutions. However, the fluoroform product will rapidly react with OH^- at higher pH conditions, and the CHF_3 and HCO_3^- are no longer observed; in their place, we see F^-, $HCOO^-$, and additional CO_3^{2-} (Figure 3). Repeated nucleophilic substitution reactions release F^-, and dehydration of the resulting unstable gem-diol yields the observed format ($HCOO^-$) product.

Although previous reports propose the formation of CO as a reaction product [43], we did not observe any CO in the gas phase, consistent with the mechanism proposed here. Alternatively, the yields were either below the detection limit, or any CO formed reacted rapidly with OH^- to yield the formate ($CO + OH^- \rightarrow HCOO^-$), which was observed in experiments with NaOH amendment. Related to the hydrothermal treatment of PFCAs, the kinetics of C_4 – C_{12} PFCAs in HALT have been previously studied in batch reactors [9]. However, these studies did not report on analyzing any gaseous species. We hypothesize that the general hydrothermal degradation reaction mechanism will hold for longer-chain PFCAs; the intermediate step in degradation pathways will yield the corresponding 1H-perfluoroalkane volatile organic fluorine species (VOFs), but the addition of NaOH will rapidly defluorinate these species to F^- and a mixture of organic and inorganic carbon species. Further work is needed to test this hypothesis and identify the range of end products for different PFCAs.

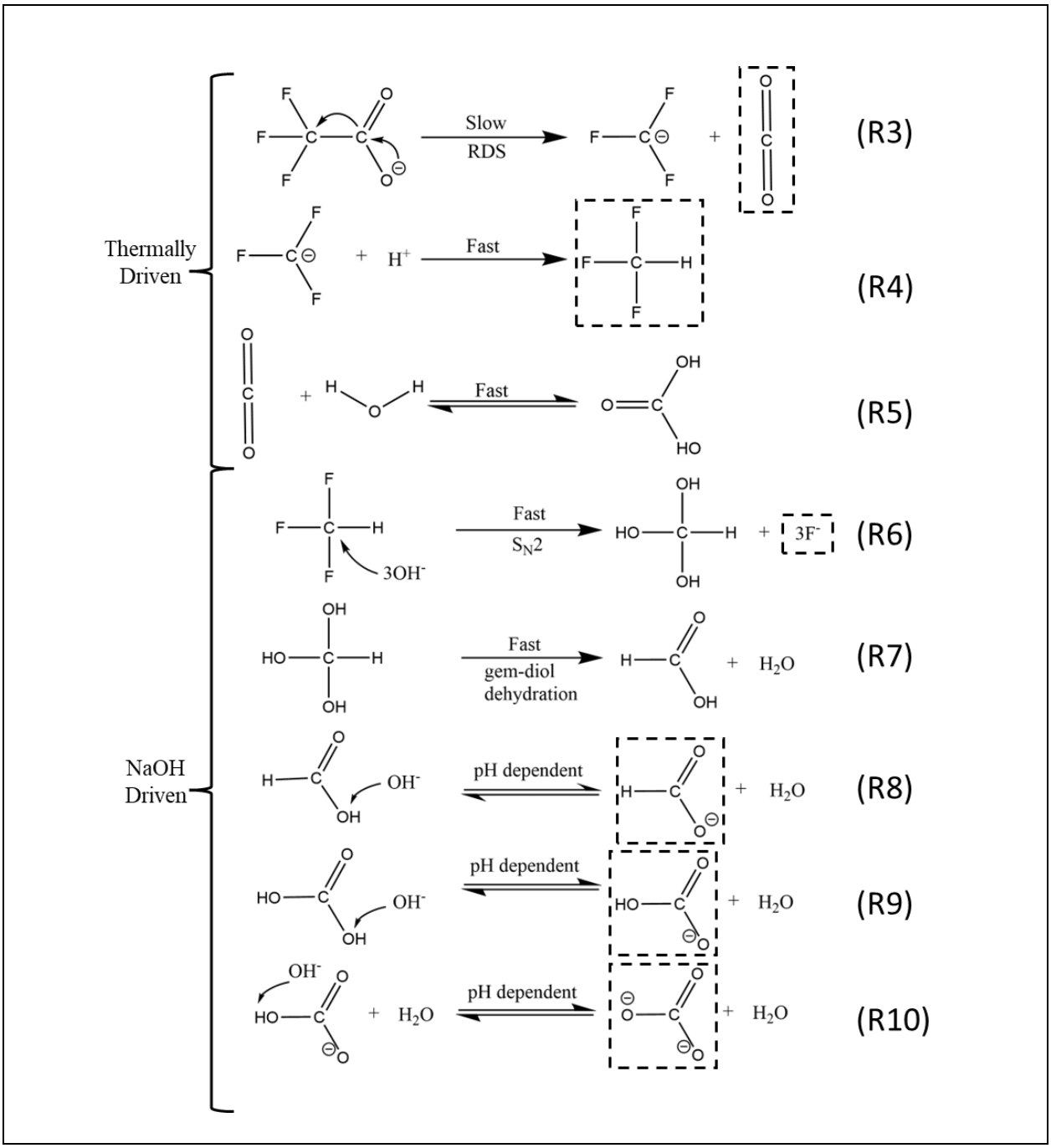

Figure 5: Proposed TFA reaction pathway for hydrothermal transformation and mineralization of TFA, Including alkali–independent and alkali–dependent reaction steps. The products inside the dash lines are observed experimentally.

The decarboxylation step of the proposed mechanism is likely generalizable to other PFCAs, e.g., in their 1950s paper, LaZerte et al. showed that PFCAs in the form $F(CF_2)_nCOOH$ degrade to $F(CF_2)_nH$ when dissolved in water or ethylene glycol at elevated temperatures. This trend does not

hold for the thermal degradation of PFCAs in gaseous form, which typically produces primary perfluoroalkanes [44]. While there is evidence of the decarboxylation pathway for PFCAs, the decomposition rates have not been reported. Additionally, the fate of these longer 1H-perfluoroalkanes in a caustic environment has not been investigated. Application of rapid analysis techniques, such as Raman and FTIR spectroscopy and the development of spectral libraries of fluorine gases [45], can elucidate the kinetic mechanism of PFAS destruction.

3.5 Environmental Implications

A continuous flow HALT system enables high-throughput treatment of TFA in the waste stream of industrial processes and environmental cleanup. TFA is one of the most abundant mass-produced perfluorinated chemicals and is also found in the environment as a byproduct of incomplete mineralization in several end-of-life PFAS approaches. Due to its simple chemical structure, TFA serves as a suitable model compound and a benchmark for other PFCA.

The study shows the importance of the hydrothermal decarboxylation route yielding the recalcitrant gas byproducts; thus, monitoring the process and ensuring these species' complete mineralization is essential. Fluoroform, as well as longer 1H-perfluoroalkanes, have been detected during hydrothermal PFAS treatment. By themselves, thermal methods (hydrothermal, SCWO, or incineration) may not be sufficient to fully degrade the gaseous products. The alkaline amendment aids the mineralization of volatile organic fluorine species, yielding dissolved fluoride as the stable end product.

Results show strong temperature dependency on destruction kinetics. The presented kinetic rates can be used to estimate process times required to achieve the required levels of destruction as a

function of reactor temperature. Such information could be used in the design of scale-up reactors and their optimization, *e.g.*, energy consumption, corrosion propensity, etc.

Spectroscopic methods used in the study Raman and FTIR allow for rapid analysis and identification of the liquid and gaseous species. Spectroscopic techniques can be utilized for in-situ process monitoring and control to ensure complete PFAS mineralization.

ASSOCIATED CONTENT

Supporting Information

Electronic supporting information contains detailed reactor schematics, Raman data, Raman calibrations, pH data, gas sampling data, LC-MS/MS details, and a complete data table.

AUTHOR INFORMATION

Corresponding Author

*ivn@uw.edu; +1 206 543-5248; ORCID [0000-0002-6347-7450]

Conflicts of Interest

The authors declare the following competing financial interest(s): BRP has a pecuniary interest in the technology reported herein, TJS holds a patent on applying the technology for PFAS treatment, and IVN submitted a patent on continuous flow control and operation hydrothermal reactors.

Author Contributions

The manuscript was written through the contributions of all authors. All authors have approved the final version of the manuscript.

Funding Sources

This work was supported by SERDP grant ER18-1501.

ACKNOWLEDGMENT

We would like to acknowledge Dr. Martin Sedilek (UW) for his help with LC/MS, Dr. Shar Sami (UW) and Luke Moser (UW) for his help with FTIR analysis, Dr. Chris Higgins (Colorado School of Mines, CSM) for advice in sampling and analysis of organic fluorine and Dr. Shubham Vyas (CSM) for discussions related to chemical kinetics.

REFERENCES

[1] R. C. Buck *et al.*, "Perfluoroalkyl and polyfluoroalkyl substances in the environment: terminology, classification, and origins," vol. 7, no. 4, pp. 513-541, 2011, doi: 10.1002/ieam.258.

[2] M. L. Brusseau, R. H. Anderson, and B. Guo, "PFAS concentrations in soils: Background levels versus contaminated sites," *Science of the Total Environment*, vol. 740, p. 140017, 2020.

[3] UNEP. "Stockholm convention on persistent organic pollutants (POPs) as amended in 2019 (Text and Annexes) United Nations Environment Programme (2019)." http://chm.pops.int/Portals/0/download.aspx?d=UNEP-POPS-COP-CONVTEXT-2021.English. (accessed.

[4] U. EPA. *Toxic Substances Control Act (TSCA) Inventory Update Reporting*.

[5] S. E. Lopez and J. Salazar, "Trifluoroacetic acid: Uses and recent applications in organic synthesis," *J. Fluorine Chem.*, vol. 156, pp. 73-100, 2013.

[6] (2017). *Pesticides Industry Sales and Usage 2008-2012 Market Estimates*.

[7] J. Li, C. Austin, S. Moore, B. R. Pinkard, and I. V. Novosselov, "PFOS destruction in a continuous supercritical water oxidation reactor," *Chem. Eng. J.*, vol. 451, p. 139063, 2023/01/01/ 2023, doi: https://doi.org/10.1016/j.cej.2022.139063.

[8] R. K. Singh, S. Fernando, S. F. Baygi, N. Multari, S. M. Thagard, and T. M. Holsen, "Breakdown products from perfluorinated alkyl substances (PFAS) degradation in a plasma-based water treatment process," *Environmental Science & Technology*, vol. 53, no. 5, pp. 2731-2738, Mar 2019, doi: 10.1021/acs.est.8b07031.

[9] J. Endo and T. Funazukuri, "Hydrothermal alkaline defluorination rate of perfluorocarboxylic acids (PFCAs)," *Journal of Chemical Technology & Biotechnology*, vol. 98, no. 5, pp. 1215-1221, 2023.

[10] M. Yang *et al.*, "Experimental and Theoretical Insight of Perfluorooctanoic Acid Destruction by Alkaline Hydrothermal Treatment Enhanced with Zero-Valent Iron in Biochar," *ACS ES&T Water*, vol. 3, no. 5, pp. 1286-1293, 2023/05/12 2023, doi: 10.1021/acsestwater.2c00614.

[11] B. Trang, Y. Li, X.-S. Xue, M. Ateia, K. Houk, and W. R. Dichtel, "Low-temperature mineralization of perfluorocarboxylic acids," *Science*, vol. 377, no. 6608, pp. 839-845, 2022.

[12] S. P. Sahu, M. Qanbarzadeh, M. Ateia, H. Torkzadeh, A. S. Maroli, and E. L. Cates, "Rapid degradation and mineralization of perfluorooctanoic acid by a new petitjeanite Bi3O (OH)(PO4) 2 microparticle ultraviolet photocatalyst," *Environmental Science & Technology Letters*, vol. 5, no. 8, pp. 533-538, 2018.

[13] S. S. Kalra *et al.*, "Sonolytic destruction of per- and polyfluoroalkyl substances in groundwater, aqueous film-forming foams, and investigation derived waste," *Chem. Eng. J.*, vol. 425, Dec 2021, Art no. 131778, doi: 10.1016/j.cej.2021.131778.

[14] S. J. Smith *et al.*, "Electrochemical Oxidation for Treatment of PFAS in Contaminated Water and Fractionated Foam─ A Pilot-Scale Study," *ACS Es&t Water*, vol. 3, no. 4, pp. 1201-1211, 2023.

[15] C. Austin, J. Li, S. Moore, A. Purohit, B. R. Pinkard, and I. V. Novosselov, "Destruction and defluorination of PFAS matrix in continuous-flow supercritical water oxidation reactor: Effect of operating temperature," *Chemosphere*, p. 138358, 2023/03/09/ 2023, doi: https://doi.org/10.1016/j.chemosphere.2023.138358.

[16] J. Li, B. R. Pinkard, S. Wang, and I. V. Novosselov, "Review: Hydrothermal treatment of per- and polyfluoroalkyl substances (PFAS)," *Chemosphere*, vol. 307, p. 135888, 2022/11/01/ 2022, doi: https://doi.org/10.1016/j.chemosphere.2022.135888.

[17] P. Beumers, T. Brands, H.-J. Koss, and A. Bardow, "Model-free calibration of Raman measurements of reactive systems: Application to monoethanolamine/water/CO2," *Fluid Phase Equilib.*, vol. 424, pp. 52-57, 2016/09/25/ 2016, doi: https://doi.org/10.1016/j.fluid.2015.10.004.

[18] B. R. Pinkard, D. J. Gorman, E. G. Rasmussen, J. C. Kramlich, P. G. Reinhall, and I. V. Novosselov, "Kinetics of formic acid decomposition in subcritical and supercritical water – a Raman spectroscopic study," *International Journal of Hydrogen Energy*, vol. 44, no. 60, pp. 31745-31756, 2019/12/06/ 2019, doi: https://doi.org/10.1016/j.ijhydene.2019.10.070.

[19] B. R. Pinkard, J. C. Kramlich, and I. V. Novosselov, "Gasification Pathways and Reaction Mechanisms of Primary Alcohols in Supercritical Water," *ACS Sustainable Chemistry & Engineering*, vol. 8, no. 11, pp. 4598-4605, 2020/03/23 2020, doi: 10.1021/acssuschemeng.0c00445.

[20] B. R. Pinkard, A. L. Purohit, S. J. Moore, J. C. Kramlich, P. G. Reinhall, and I. V. Novosselov, "Partial Oxidation of Ethanol in Supercritical Water," *Industrial & Engineering Chemistry Research*, vol. 59, no. 21, pp. 9900-9911, 2020/05/27 2020, doi: 10.1021/acs.iecr.0c00945.

[21] B. R. Pinkard, S. Shetty, J. C. Kramlich, P. G. Reinhall, and I. V. Novosselov, "Hydrolysis of Dimethyl Methylphosphonate (DMMP) in Hot-Compressed Water," *The Journal of Physical Chemistry A*, vol. 124, no. 41, pp. 8383-8389, 2020/10/15 2020, doi: 10.1021/acs.jpca.0c05104.

[22] B. R. Pinkard *et al.*, "Raman Spectroscopic Data from Formic Acid Decomposition in Subcritical and Supercritical Water," *Data in Brief*, p. 105312, 2020.

[23] H. Hori, Y. Nagaoka, T. Sano, and S. Kutsuna, "Iron-induced decomposition of perfluorohexanesulfonate in sub- and supercritical water," *Chemosphere*, vol. 70, no. 5, pp. 800-806, Jan 2008, doi: 10.1016/j.chemosphere.2007.07.015.

[24] B. R. Wu, S. L. Hao, Y. J. Choi, C. P. Higgins, R. Deeb, and T. J. Strathmann, "Rapid Destruction and Defluorination of Perfluorooctanesulfonate by Alkaline Hydrothermal

Reaction," *Environmental Science & Technology Letters*, vol. 6, no. 10, pp. 630-636, Oct 2019, doi: 10.1021/acs.estlett.9b00506.
[25] B. R. Pinkard, S. Shetty, D. Stritzinger, C. Bellona, and I. V. Novosselov, "Destruction of perfluorooctanesulfonate (PFOS) in a batch supercritical water oxidation reactor," *Chemosphere*, vol. 279, Sep 2021, Art no. 130834, doi: 10.1016/j.chemosphere.2021.130834.
[26] B. R. Pinkard, "Aqueous film-forming foam treatment under alkaline hydrothermal conditions," *Journal of Environmental Engineering*, vol. 148, no. 2, p. 05021007, 2022.
[27] S. Hao, Y.-J. Choi, B. Wu, C. P. Higgins, R. Deeb, and T. J. Strathmann, "Hydrothermal Alkaline Treatment for Destruction of Per- and Polyfluoroalkyl Substances in Aqueous Film-Forming Foam," *Environmental Science & Technology*, vol. 55, no. 5, pp. 3283-3295, 2021/03/02 2021, doi: 10.1021/acs.est.0c06906.
[28] O. Soker, S. Hao, B. G. Trewyn, C. P. Higgins, and T. J. Strathmann, "Application of Hydrothermal Alkaline Treatment to Spent Granular Activated Carbon: Destruction of Adsorbed PFASs and Adsorbent Regeneration," *Environmental Science & Technology Letters*, vol. 10, no. 5, pp. 425-430, 2023/05/09 2023, doi: 10.1021/acs.estlett.3c00161.
[29] S. Hao, Y. J. Choi, R. A. Deeb, T. J. Strathmann, and C. P. Higgins, "Application of Hydrothermal Alkaline Treatment for Destruction of Per- and Polyfluoroalkyl Substances in Contaminated Groundwater and Soil," *Environmental Science & Technology*, vol. 56, no. 10, pp. 6647-6657, 2022/05/17 2022, doi: 10.1021/acs.est.2c00654.
[30] S. Hao *et al.*, "Hydrothermal Alkaline Treatment (HALT) of Foam Fractionation Concentrate Derived from PFAS-Contaminated Groundwater," *Environmental Science & Technology*, vol. 57, no. 44, pp. 17154-17165, 2023/11/07 2023, doi: 10.1021/acs.est.3c05140.
[31] B. R. Pinkard, C. Austin, A. L. Purohit, J. Li, and I. V. Novosselov, "Destruction of PFAS in AFFF-impacted fire training pit water, with a continuous hydrothermal alkaline treatment reactor," *Chemosphere*, vol. 314, p. 137681, 2023/02/01/ 2023, doi: https://doi.org/10.1016/j.chemosphere.2022.137681.
[32] B. R. Pinkard, D. J. Gorman, K. Tiwari, J. C. Kramlich, P. G. Reinhall, and I. V. Novosselov, "Review of Gasification of Organic Compounds in Continuous-Flow, Supercritical Water Reactors," *Industrial & Engineering Chemistry Research*, vol. 57, no. 10, pp. 3471-3481, 2018.
[33] B. R. Pinkard, S. Shetty, D. Stritzinger, C. Bellona, and I. V. Novosselov, "Destruction of perfluorooctanesulfonate (PFOS) in a batch supercritical water oxidation reactor," *Chemosphere*, vol. 279, p. 130834, 2021/09/01/ 2021, doi: https://doi.org/10.1016/j.chemosphere.2021.130834.
[34] E. G. Rasmussen, J. Kramlich, and I. V. Novosselov, "Scalable Continuous Flow Metal–Organic Framework (MOF) Synthesis Using Supercritical CO2," *ACS Sustainable Chemistry & Engineering*, vol. 8, no. 26, pp. 9680-9689, 2020/07/06 2020, doi: 10.1021/acssuschemeng.0c01429.
[35] H. S. Fogler, *Essentials of chemical reaction engineering: essenti chemica reactio engi*. Pearson Education, 2010.
[36] A. Vakulka, G. Tavčar, and T. Skapin, "Interaction of trifluoromethane (CHF3) with alkali hydroxides and carbonates," *J. Fluorine Chem.*, vol. 142, pp. 52-59, 2012.
[37] F. M. Miloserdov and V. V. Grushin, "Alcoholysis of fluoroform," *J. Fluorine Chem.*, vol. 167, pp. 105-109, 2014.

[38] I. Auerbach, F. H. Verhoek, and A. L. Henne, "Kinetic studies on the decarboxylation of sodium trifluoroacetate in ethylene glycol," *Journal of the American Chemical Society*, vol. 72, no. 1, pp. 299-300, 1950.

[39] A. J. Belsky, P. G. Maiella, and T. B. Brill, "Spectroscopy of Hydrothermal Reactions 13. Kinetics and Mechanisms of Decarboxylation of Acetic Acid Derivatives at 100−260 °C under 275 bar," *The Journal of Physical Chemistry A*, vol. 103, no. 21, pp. 4253-4260, 1999/05/01 1999, doi: 10.1021/jp984122d.

[40] J. Schoppelrei, M. Kieke, X. Wang, M. Klein, and T. Brill, "Spectroscopy of hydrothermal reactions. 4. Kinetics of urea and guanidinium nitrate at 200− 300 C in a diamond cell, infrared spectroscopy flow reactor," *The Journal of Physical Chemistry*, vol. 100, no. 34, pp. 14343-14351, 1996.

[41] E. Tschuikow-Roux and J. E. Marte, "Thermal Decomposition of Fluoroform in a Single-Pulse Shock Tube. I," *The Journal of Chemical Physics*, vol. 42, no. 6, pp. 2049-2056, 2004, doi: 10.1063/1.1696246.

[42] H. Onoda, T. Ohta, J. Tamaki, and K. Kojima, "Decomposition of trifluoromethane over nickel pyrophosphate catalysts containing metal cation," *Applied Catalysis A: General*, vol. 288, no. 1, pp. 98-103, 2005/07/15/ 2005, doi: https://doi.org/10.1016/j.apcata.2005.04.028.

[43] A. V. Patwardhan and M. M. Sharma, "Kinetics of absorption of carbon monoxide in aqueous solutions of sodium hydroxide and aqueous calcium hydroxide slurries," *Industrial & Engineering Chemistry Research*, vol. 28, no. 1, pp. 5-9, 1989/01/01 1989, doi: 10.1021/ie00085a002.

[44] J. D. LaZerte, L. J. Hals, T. S. Reid, and G. H. Smith, "Pyrolyses of the Salts of the Perfluoro Carboxylic Acids," *Journal of the American Chemical Society*, vol. 75, no. 18, pp. 4525-4528, 1953.

[45] T. J. Baker *et al.*, "An infrared spectral database for gas-phase quantitation of volatile per- and polyfluoroalkyl substances (PFAS)," *Journal of Quantitative Spectroscopy and Radiative Transfer*, vol. 295, p. 108420, 2023.

Supporting Information for:

Hydrothermal destruction and defluorination of trifluoroacetic acid (TFA)

*Conrad Austin [a,b], Anmol L. Purohit [a], Cody Thomsen [a, b], Brian R. Pinkard [a, b], Timothy J. Strathmann [c], Igor V. Novosselov [a] **

[a] University of Washington, Mechanical Engineering Department, Seattle, WA 98195

[b] Aquagga, Inc., Tacoma, WA 98402

[c] Colorado School of Mines, Civil and Environmental Engineering Department, Golden, CO 80401

* Corresponding Author: ivn@uw.edu; +1 206 543-5248

ORCID [0000-0002-6347-7450]

Contents

4 Figures

4.1 Figure S1: Process diagram for Reactor 1

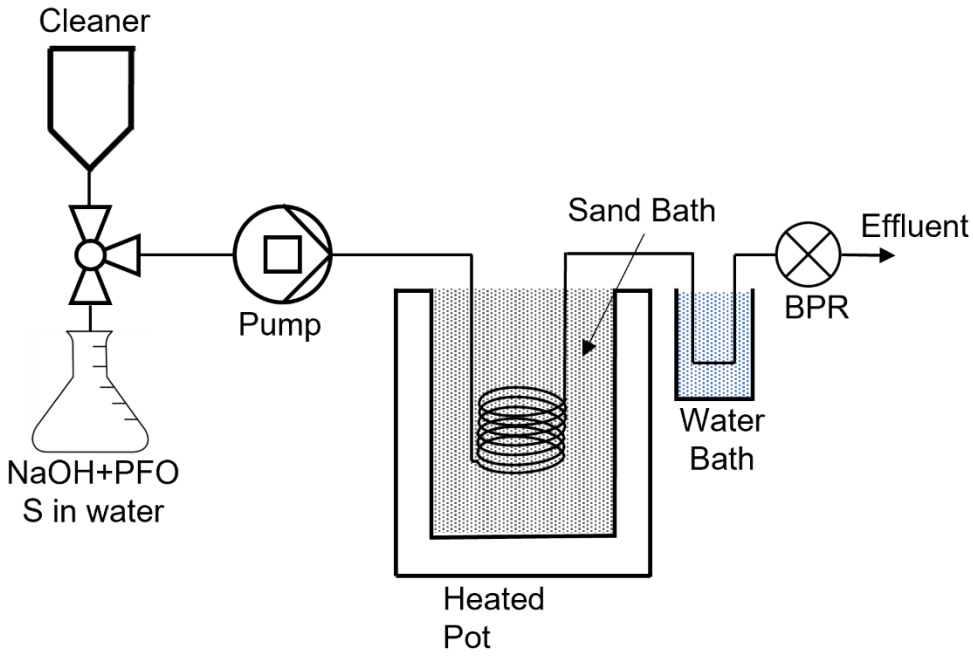

4.2 Figure S2: Process Diagram Schematic of Reactor 2. Heat exchanger is added for heat recovery

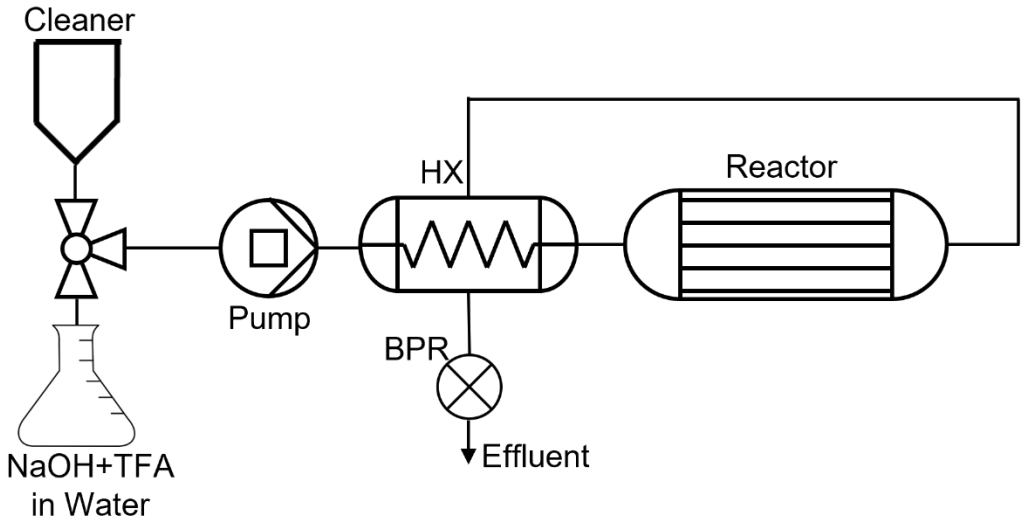

Figure S3: Photograph of Reactor 1, before the insulation and sand are added.

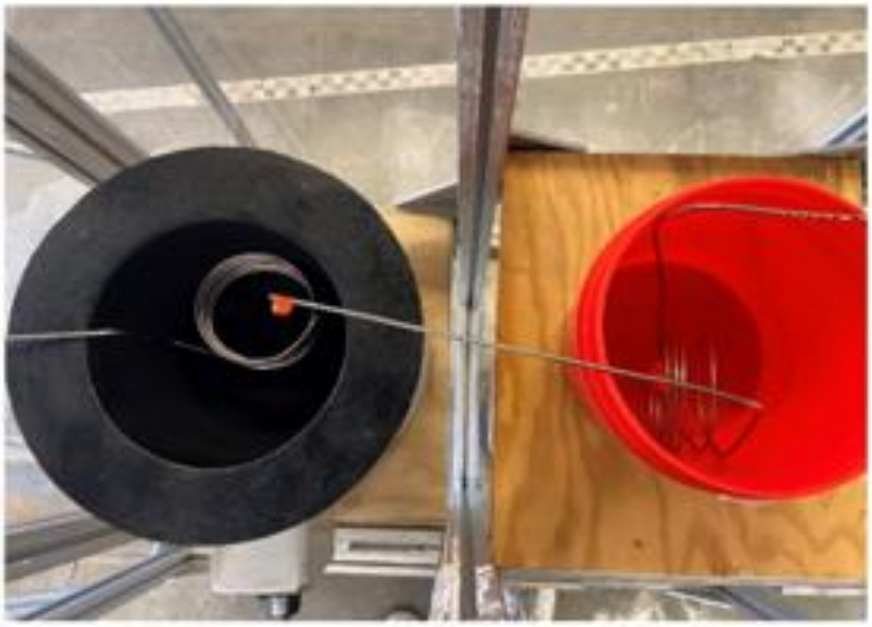

4.3 Figure S4: Picture of Reactor 2, before band heaters and insulation were added.

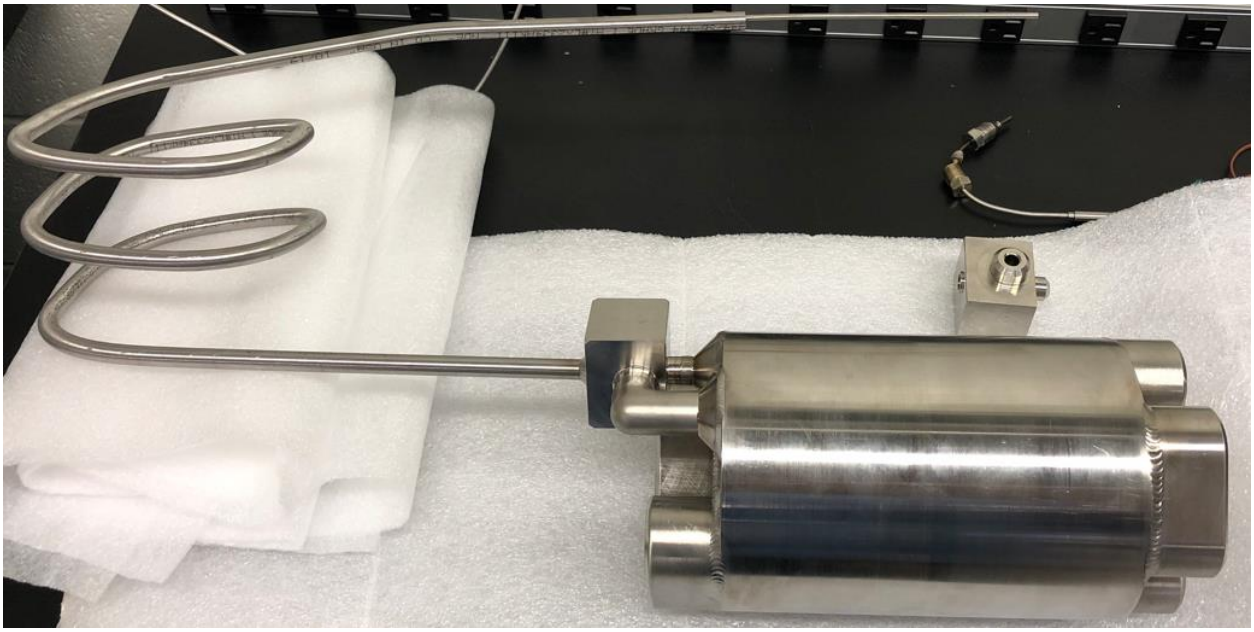

Figure S5: Example of Raman deconvolution. Conditions: T=200C, Residence time = 20min, NaOH 0.4M. Note that the raw count has been shifted up 800 units for presentation purposes. The sapphire signal is present, as the immersion Raman probe uses the Sapphire lens.

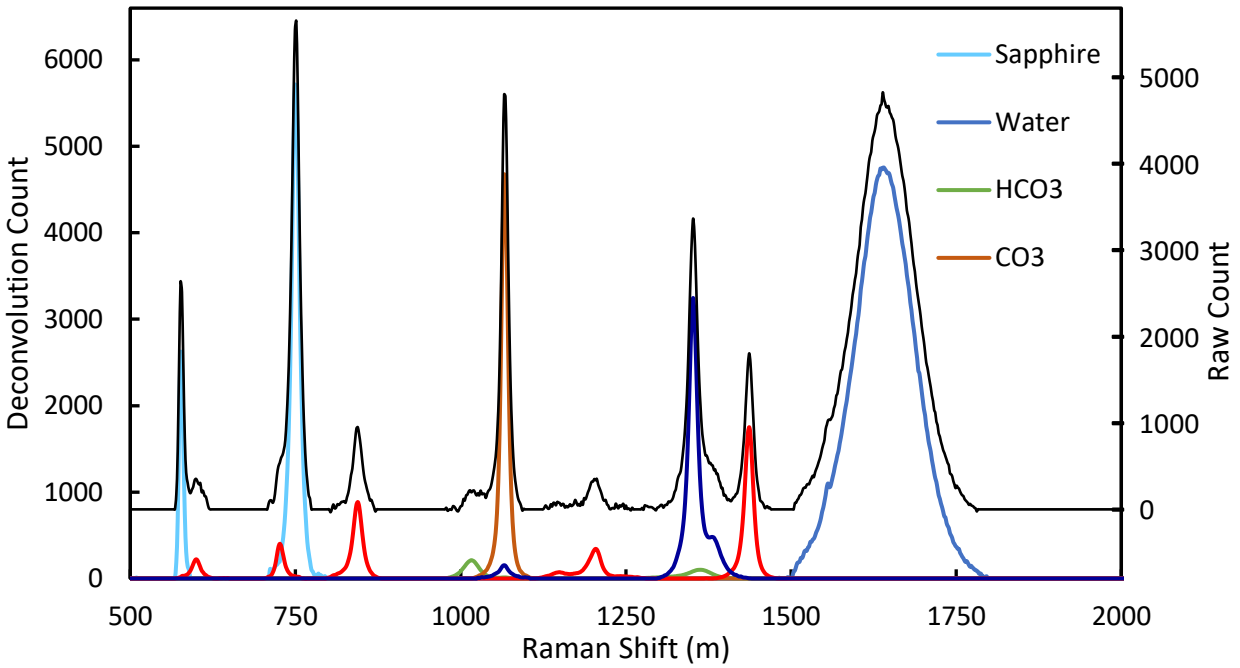

4.4 Figure S6: Raman Calibration Curves for all quantitatively measured species

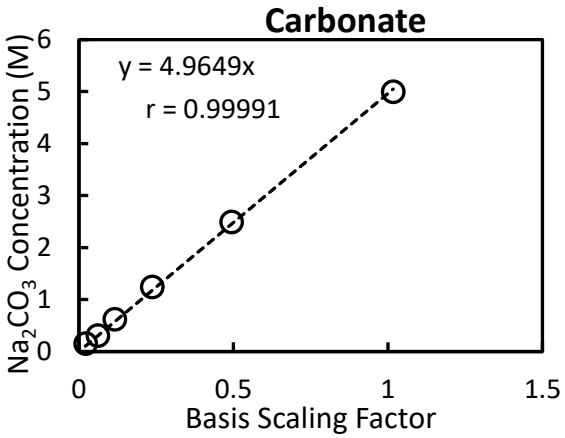

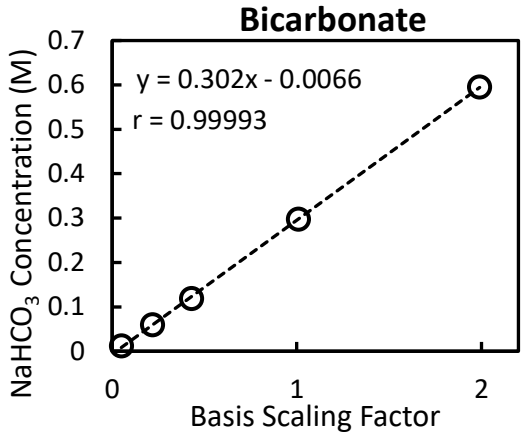

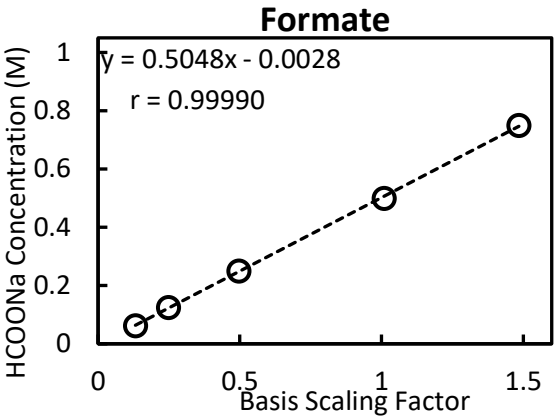

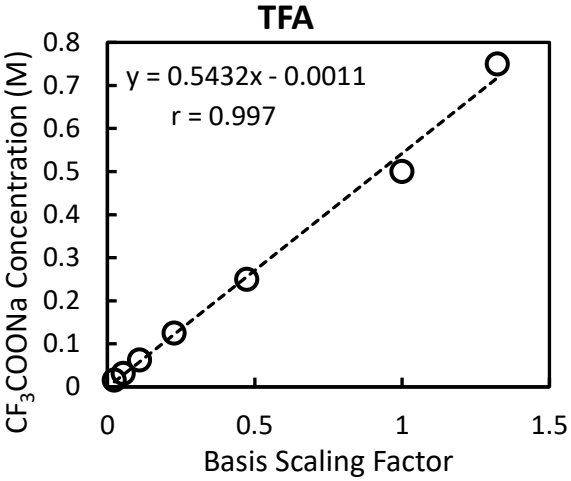

Figure S7: pH of 0.1M TFA samples treated at 200 °C.

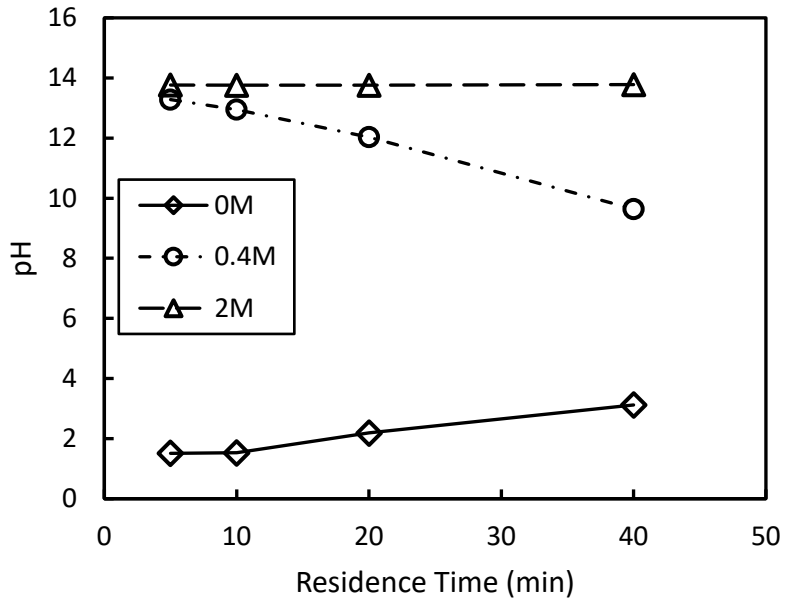

4.5 Figure S8: P-trap based Gas Sampling system of effluent stream. Argon used as a dilutent.

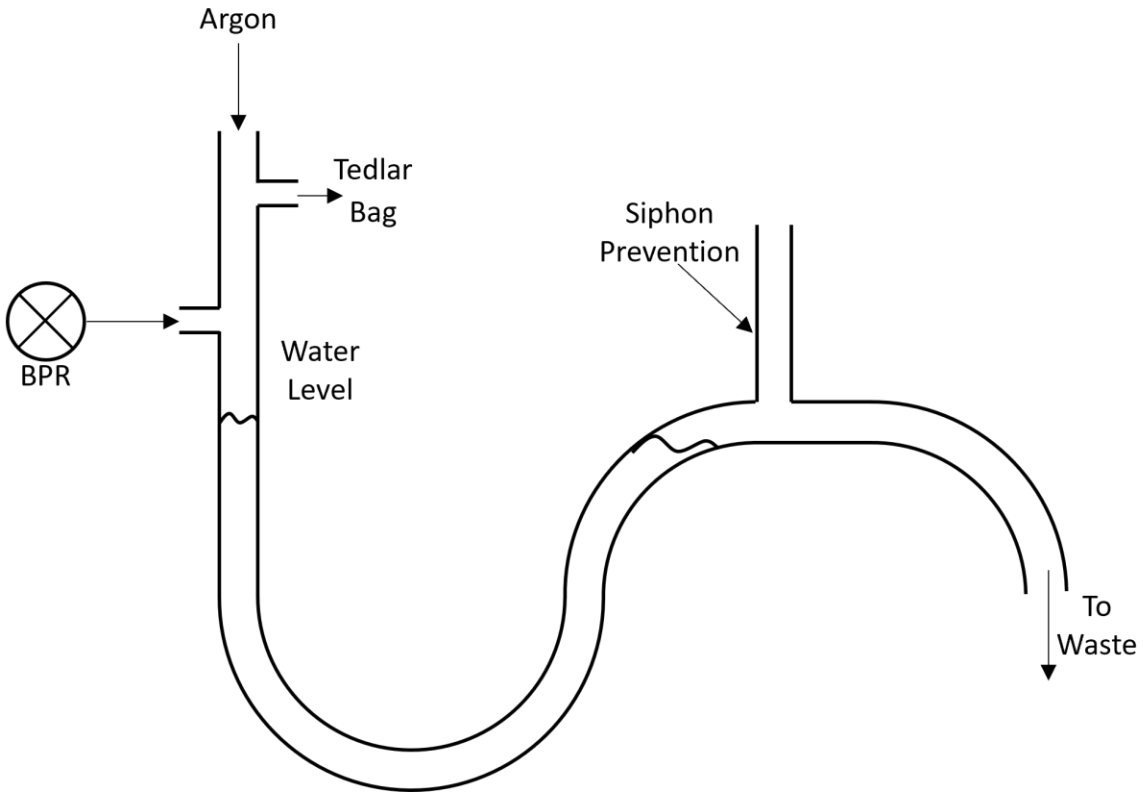

4.6 Figure S9: Raman and LC-MS/MS Comparison

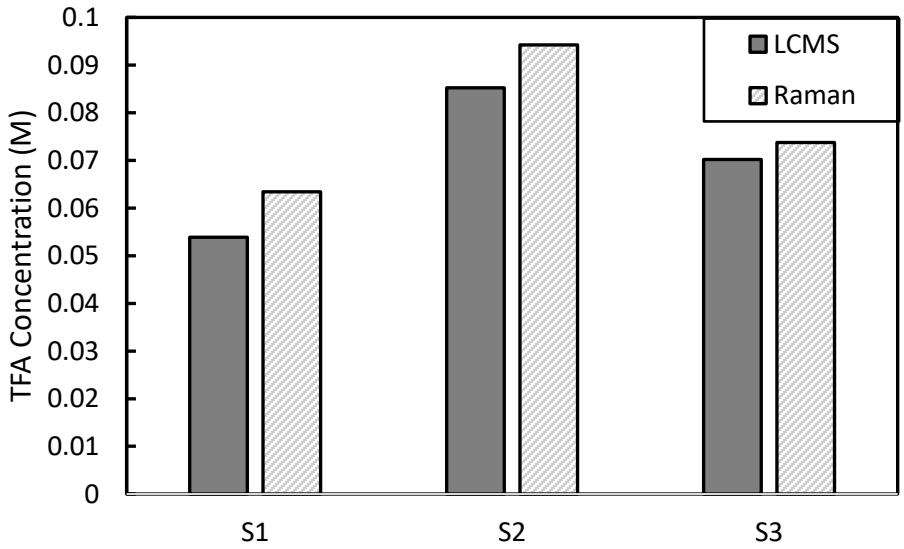

4.7 Figure S10: LC-MS/MS Details

5 Equations

5.1 Equation S1: Standard error of Slope

$$SE(\beta_1)\sqrt{\frac{1}{n-2}*\frac{\sum(y_i-\hat{y})^2}{\sum(x_i-\bar{x})^2}} \quad (S1)$$

5.2 Equation S2: Standard error of y-intercept

$$SE(\beta_0)=\sqrt{\left(\frac{1}{n-2}\right)\sum(y_i-\hat{y})^2\left[\frac{1}{n}+\frac{\bar{x}^2}{\sum(x_i-\bar{x})^2}\right]} \quad (S2)$$

6 Tables

6.1 Table S1: Full data table

NaOH (M)	Temp (C)	Res (min)	$[CF_3COO^-]_0$	$[CF_3COO^-]$	$[CO_3^{2-}]$	$[HCO_3^-]$	$[HCOO^-]$	F^-
0.0	185	40	0.102	0.085	0.000	0.000	0.000	-
0.0	193	10	0.096	0.091	0.000	0.000	0.000	-
0.0	198	5	0.096	0.088	0.000	0.000	0.000	0.000
0.0	203	10	0.096	0.074	0.000	0.000	0.000	0.001
0.0	206	20	0.096	0.047	0.000	0.000	0.000	0.001
0.0	206	40	0.096	0.013	0.000	0.000	0.000	0.003
0.0	205	5	0.096	0.079	0.000	0.000	0.000	-
0.0	213	10	0.096	0.054	0.000	0.000	0.000	-
0.0	220	5	0.102	0.047	0.000	0.000	0.000	-
0.4	178	10	0.106	0.105	0.008	0.000	0.000	-
0.4	181	20	0.106	0.094	0.018	0.000	0.010	-
0.4	182	40	0.106	0.091	0.030	0.000	0.019	-
0.4	193	5	0.106	0.094	0.015	0.000	0.007	0.027
0.4	204	10	0.106	0.063	0.049	0.000	0.041	0.147
0.4	206	20	0.106	0.038	0.068	0.012	0.064	0.217
0.4	207	40	0.106	0.007	0.010	0.094	0.078	0.284
0.4	213	10	0.106	0.032	0.063	0.012	0.061	-
0.4	220	5	0.106	0.024	0.049	0.039	0.066	-

2.0	180	40	0.088	0.118	0.036	0.000	0.028	-
2.0	195	20	0.077	0.118	0.037	0.000	0.031	-
2.0	200	5	0.102	0.118	0.015	0.000	0.013	0.058
2.0	205	10	0.075	0.118	0.043	0.000	0.039	0.154
2.0	205	20	0.046	0.118	0.070	0.000	0.066	0.260
2.0	205	40	0.015	0.118	0.108	0.000	0.097	0.334
2.0	215	10	0.041	0.118	0.075	0.000	0.071	-
2.0	225	5	0.037	0.118	0.082	0.000	0.079	-